JACS
JOURNAL OF THE AMERICAN CHEMICAL SOCIETY

Article

pubs.acs.org/JACS

# Co(salophen)-Catalyzed Aerobic Oxidation of *p*-Hydroquinone: Mechanism and Implications for Aerobic Oxidation Catalysis

Colin W. Anson,[†] Soumya Ghosh,[‡] Sharon Hammes-Schiffer,*[,‡] and Shannon S. Stahl*[,†]

[†]Department of Chemistry, University of Wisconsin—Madison, 1101 University Avenue, Madison, Wisconsin 53706, United States
[‡]Department of Chemistry, University of Illinois at Urbana−Champaign, 600 South Mathews Avenue, Urbana, Illinois 61801, United States

Supporting Information

**ABSTRACT:** Macrocyclic metal complexes and *p*-benzoquinones are commonly used as co-catalytic redox mediators in aerobic oxidation reactions. In an effort to gain insight into the mechanism and energetic efficiency of these reactions, we investigated Co(salophen)-catalyzed aerobic oxidation of *p*-hydroquinone. Kinetic and spectroscopic data suggest that the catalyst resting-state consists of an equilibrium between a $Co^{II}$(salophen) complex, a $Co^{III}$-superoxide adduct, and a hydrogen-bonded adduct between the hydroquinone and the $Co^{III}-O_2$ species. The kinetic data, together with density functional theory computational results, reveal that the turnover-limiting step involves proton-coupled electron transfer from a semi-hydroquinone species and a $Co^{III}$-hydroperoxide intermediate. Additional experimental and computational data suggest that a coordinated $H_2O_2$ intermediate oxidizes a second equivalent of hydroquinone. Collectively, the results show how Co(salophen) and *p*-hydroquinone operate synergistically to mediate $O_2$ reduction and generate the reactive *p*-benzoquinone co-catalyst.

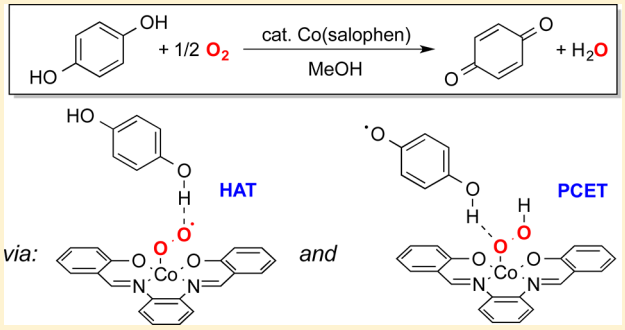


## INTRODUCTION

Homogeneous metal-catalyzed aerobic oxidation reactions are the focus of extensive study.[1] Many of these reactions proceed via an "oxidase"-type mechanism[1a] involving two independent half-reactions: (1) oxidation of the organic molecule mediated by the oxidized catalyst and (2) oxidation of the reduced catalyst by $O_2$. Co-catalytic redox mediators are often used to facilitate the use of $O_2$ as the terminal oxidant. This approach is commonly featured in Pd-catalyzed oxidation reactions, in which benzoquinones and macrocyclic Co or Fe complexes have been used as mediators in a wide range of organic oxidation reactions (Scheme 1),[1c,2,3] including Wacker-type oxidation of alkenes,[3a] allylic acetoxylation,[3b] 1,4-oxidative difunctionalization of conjugated dienes,[3c] and oxidative C−C coupling reactions.[3d] Metal-macrocycle/quinone co-catalyst systems have also been used in other reactions, such as Ru-catalyzed alcohol and amine oxidations,[4a,b] and quinone-catalyzed dehydrogenation and dehydrogenative coupling of amines.[4c,d]

In spite of the widespread use of metal-macrocycle/quinone co-catalyst systems, relatively little is known about the mechanism of aerobic oxidation of hydroquinones mediated by metal macrocycles (cf. shaded cycle in Scheme 1). Insights into this process have implications not only for aerobic oxidation of organic molecules, but also for biological energy transduction,[5] which commonly features quinone mediators, and for energy-conversion technologies that require efficient reduction of $O_2$ to water.[6]

**Scheme 1. Example of Coupled Redox Cycles Employing Metal-Macrocycle and Hydroquinone Mediators in Pd-Catalyzed Allylic Acetoxylation**

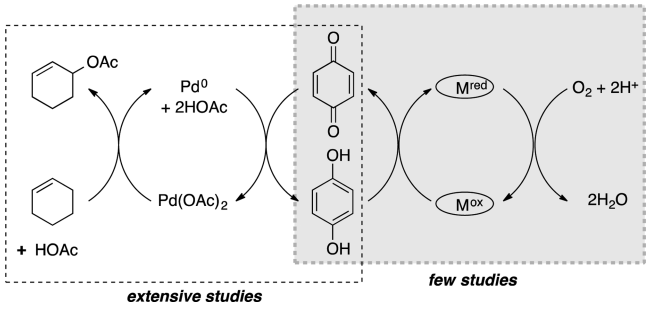


Co(salophen) is one of the most common co-catalysts used in Pd-based and other catalytic aerobic oxidation reactions.[1c,3c,e,4d] The mechanism of cobalt-catalyzed aerobic oxidation of hydroquinones has been studied predominantly with catechol substrates (i.e., *o*-hydroquinones), such as 3,5-di-*tert*-butylcatechol,[7,8] because of the relationship of this reaction to catechol oxidase and related enzymatic reactions. The

**Received:** January 8, 2016
**Published:** February 29, 2016





DOI: 10.1021/jacs.6b00254
J. Am. Chem. Soc. 2016, 138, 4186−4193

relevance of these studies to the oxidation of *p*-hydroquinone ($H_2Q$) to *p*-benzoquinone (BQ) is not clear, however, because catechols commonly chelate the metal center, and this coordination mode is not accessible to $H_2Q$.[9] The studies of Co(salophen)-catalyzed aerobic oxidation of $H_2Q$ presented in eq 1 validate this distinction and provide kinetic, spectroscopic,

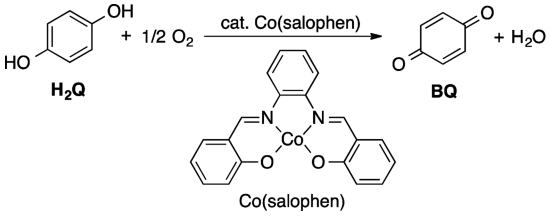


(1)

and computational insights into the mechanism of the reaction. The results highlight the role of H-atom and proton-coupled electron transfer (PCET)[10] steps in the $O_2$ reduction sequence and suggest that hydroquinones could help to avoid unselective side reactions in aerobic oxidation reactions by serving as "anti-oxidants" that intercept reactive oxygen species.

## RESULTS AND DISCUSSION

**Kinetic Studies of $H_2Q$ Oxidation by Co(salophen).** Co(salophen)-catalyzed aerobic oxidation of $H_2Q$ (eq 1) proceeds effectively in a number of different solvents, including MeOH, DMF, THF, $CH_3CN$ and AcOH (Figure 1); however, the reaction in MeOH is particularly efficient, proceeding approximately 40-fold faster than in DMF. Subsequent studies therefore employed MeOH as the solvent. Analysis of the reaction stoichiometry shows that $H_2Q$ and $O_2$ are consumed in a 2:1 ratio, as shown in eq 1, indicating that $O_2$ is fully reduced to water. Control experiments showed that oxidation of hydroquinone does not occur in the absence of Co-(salophen). A heterogeneous Co source ($Co_3O_4$) and simple $Co^{II}$ salts [$Co(acac)_2$, $Co(OAc)_2{\cdot}4H_2O$] are not effective catalysts for $H_2Q$ oxidation under similar conditions, while Co(salen) shows similar activity to Co(salophen) (Figure S1). Co(tetraphenylporphyrin) is not sufficiently soluble in MeOH to assess its comparative reactivity.

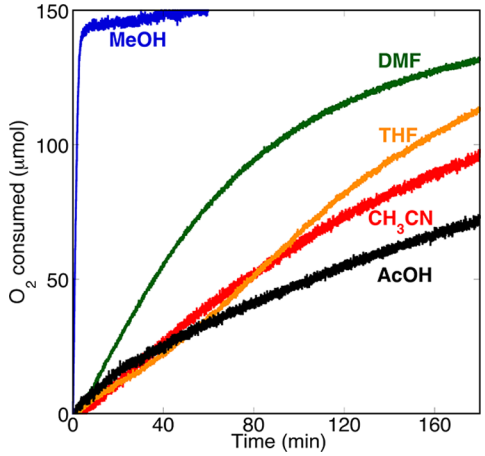


**Figure 1.** Time course data for the catalytic oxidation of hydroquinone with Co(salophen) measured by gas uptake. Reaction conditions: [Co(salophen)], 6.7 mM; [$H_2Q$], 133 mM; $pO_2$, 530 Torr; $T$ = 27 °C; solution volume, 2.25 mL; solvent, methanol (blue), DMF (green), THF (orange), $CH_3CN$ (red), or AcOH (black).

The dependence of the reaction rate on each of the reaction components [Co(salophen), $H_2Q$, and $O_2$] was then analyzed by monitoring the rate of $O_2$ consumption using a computer-interfaced gas-uptake apparatus. The reactions exhibited well-behaved time courses (Figures S2–S4) that enabled the kinetics to be probed by initial-rate methods. The kinetic data (Figure 2) reveal that the reaction exhibits a first-order dependence on [Co(salophen)] at ≤2.7 mM. At higher concentrations, the reaction rate is limited by the rate of $O_2$ mass-transfer into solution. Control experiments, for example, show that the rate is dependent on the stir-rate at high [Co], while no stir-rate dependence is observed at low [Co] (see Supporting Information, section V). To avoid complications associated with $O_2$ mass transfer, all other kinetic studies were performed with 1.8 mM Co(salophen) to ensure that the rate of BQ formation did not exceed 30 mM/min. Under these conditions, the reaction exhibits a saturation kinetic dependence on both the $O_2$ pressure ($pO_2$) and [$H_2Q$]. A significant deuterium kinetic isotope effect was observed upon comparison of the rates of reactions performed in MeOH and MeOD: $k_H/k_D$ = 4.0 ± 0.5 (Figure S7).[11]

**Spectroscopic Studies of $H_2Q$ Oxidation by Co-(salophen).** UV–visible and EPR spectroscopic studies were performed to gain a better understanding of the interaction between the different catalyst components and the identity of the catalyst resting state.

*EPR Spectroscopic Studies of $Co^{II}$(salophen).* $Co^{II}$(salophen) dissolved in MeOH under anaerobic conditions (recorded at 10 K) exhibits a relatively complex EPR spectrum (Figure 3A). Two low-spin $Co^{II}$ signals with hyperfine coupling to Co are present, together with a broad high-spin $Co^{II}$ signal at lower field (approximately 1500 G). Analogous mixtures of high- and low-spin $Co^{II}$ species have been characterized previously with $Co^{II}$(salen) complexes in protic solvent mixtures (e.g., AcOH/toluene),[12] and density functional theory (DFT) computations indicate that the $S$ = 1/2 and 3/2 spin states for $Co^{II}$(salophen) complexes bearing one or two axial methanol ligands are similar in free energy (see Supporting Information, section XV). The two low-spin signals are tentatively attributed to complexes with slight variations in their axial ligands (e.g., one vs two methanol ligands).[12,13] The EPR spectrum simplifies for $Co^{II}$(salophen) dissolved in a 1:1 mixture of MeOH:DMF, wherein a single low-spin $Co^{II}$ species is dominant, although the high-spin species is still evident (Figure 3B).

*UV–Visible and EPR Spectroscopic Analysis of $Co^{II}$(salophen) in the Presence of $O_2$.* $O_2$ gas was bubbled through a MeOH solution of $Co^{II}$(salophen) in an EPR tube for 1–2 min at room temperature, after which the solution was frozen in liquid $N_2$. An EPR spectrum of this sample reveals that the low-spin $Co^{II}$ signal is no longer present and is replaced by a new signal consistent with a $Co^{III}$-superoxide species (Figure 4A). The spectrum of this species resembles that of similar complexes reported previously in the literature (for comparisons, see Table S6).[14] A high-spin $Co^{II}$ signal is still present in this spectrum. If the experiment is performed in a 1:1 mixture of MeOH:DMF (Figure 4B), only the $Co^{III}$-superoxide species is evident in the spectrum. When the solution of $Co^{II}$(salophen) in MeOH is exposed to $O_2$ for extended periods (e.g., >10 min) before freezing in liquid $N_2$, no EPR signal is observed. This outcome is consistent with autoxidation of $Co^{II}$ to $Co^{III}$ (eq 2), which has been studied previously for Co(salen) and other $Co^{II}$/Schiff base complexes in MeOH.[15,16]


DOI: 10.1021/jacs.6b00254
J. Am. Chem. Soc. 2016, 138, 4186–4193

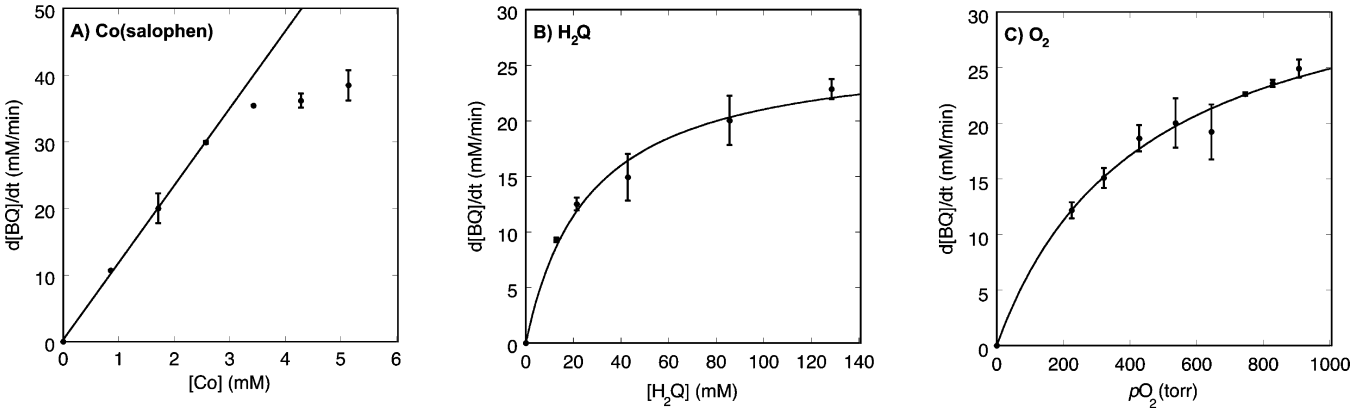


**Figure 2.** Kinetic data for Co(salophen)-catalyzed aerobic oxidation of hydroquinone: dependencies on [Co(salophen)] (A), [$H_2Q$] (B), and $pO_2$ (C) measured via initial rates. Standard conditions: [Co(salophen)], 1.7 mM; [$H_2Q$], 86 mM; $pO_2$, 530 Torr $O_2$; T = 27 °C; solution volume, 3.5 mL MeOH.

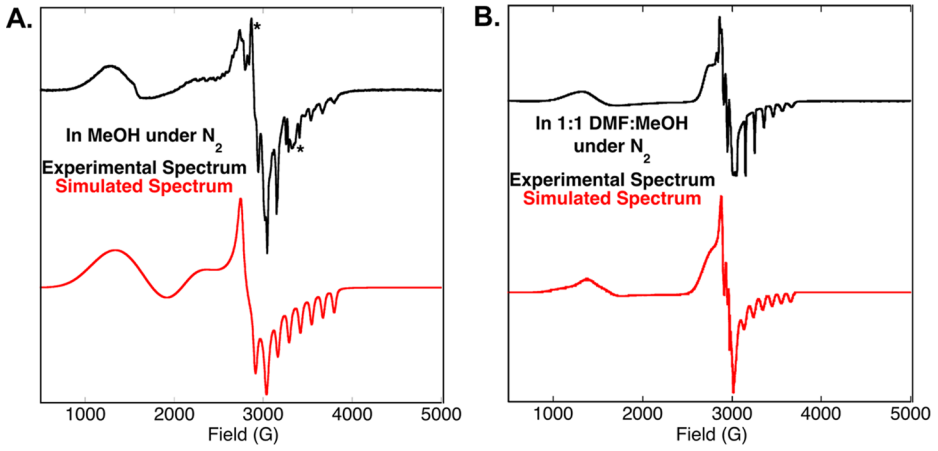


**Figure 3.** (A) EPR spectrum and simulation of a frozen solution of $Co^{II}$(salophen) in MeOH under $N_2$, revealing a high-spin $Co^{II}$ signal and two low-spin $Co^{II}$ signals. Parameters for the major low-spin species: $g$ = 3.053, 2.35, 2.025; $A$ = 125, 110, 360 MHz. The asterisks (*) denote the signals associated with the minor low-spin species. (B) EPR spectrum and simulation of a frozen solution of $Co^{II}$(salophen) in a 1:1 mixture of DMF and MeOH under $N_2$. The signal due to the high-spin species is substantially reduced relative to the spectrum in MeOH, with the main signal arising from a low-spin $Co^{II}$ species, which has the following EPR parameters: $g$ = 2.455, 2.272, 2.061; $A$ = 10, 20, 300 MHz. Comparison of $g$ and $A$ values for $Co^{II}$(salophen) under these conditions to literature examples is given in Table S5.

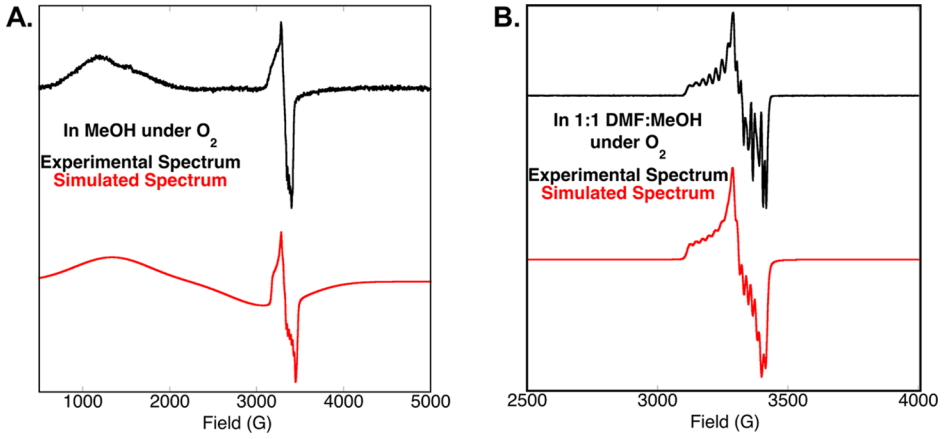


**Figure 4.** (A) EPR spectrum and simulation of a frozen solution of $Co^{II}$(salophen) in MeOH under $O_2$ (1 atm), revealing $Co^{III}$-superoxide and high-spin $Co^{II}$ signals. Parameters for the $Co^{III}$-superoxide species: $g$ = 2.095, 2.016, 1.995; $A$ = 50, 60, 50 MHz. (B) EPR spectrum and simulation of a frozen solution of $Co^{II}$(salophen) dissolved in a 1:1 mixture of DMF and MeOH under $O_2$ (1 atm). A $Co^{III}$-superoxide is the only species observed and has the following EPR parameters: $g$ = 2.023, 2.023, 2.115; $A$ = 48, 33, 72 MHz. Comparison of $g$ and $A$ values for related $Co^{III}$-superoxide species is given in Table S6.



DOI: 10.1021/jacs.6b00254
J. Am. Chem. Soc. 2016, 138, 4186−4193

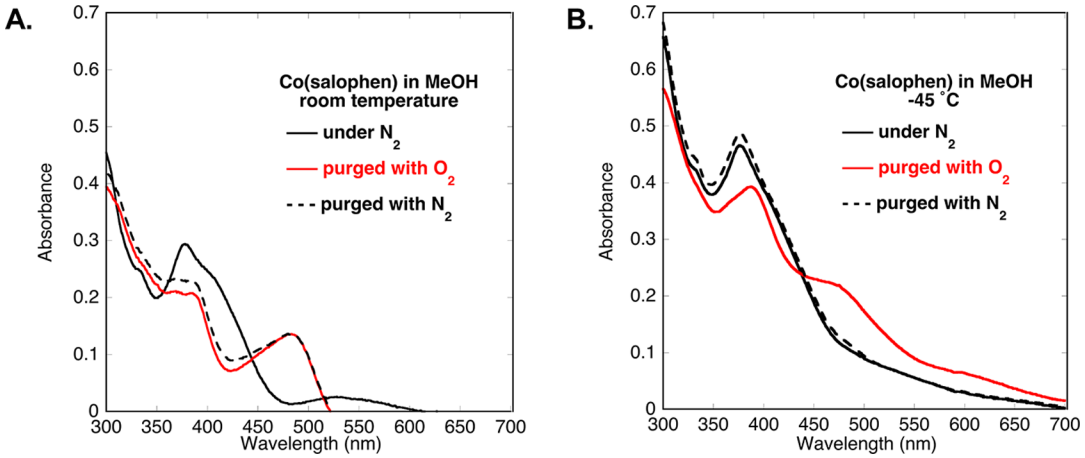


**Figure 5.** (A) UV−visible spectra of $Co^{II}$(salophen) dissolved in MeOH at room temperature under $N_2$ (solid black), after bubbling $O_2$ through the solution (solid red), and then after sparging the solution with $N_2$ (dashed black line). (B) UV−visible spectra of $Co^{II}$(salophen) dissolved in MeOH at −45 °C under $N_2$ (solid black), after bubbling $O_2$ through the solution (solid red), and then after sparging the solution with $N_2$ (dashed black line). Conditions: 0.1 mM Co, 1 atm $O_2$ or $N_2$, MeOH, room temperature or −45 °C.

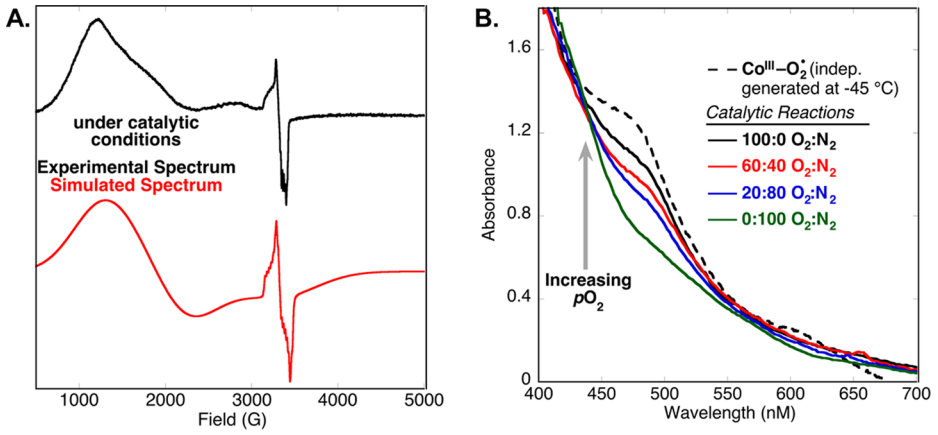


**Figure 6.** (A) EPR spectrum and simulation of a frozen solution of the catalytic reaction mixture [$Co^{II}$(salophen) + $H_2Q$ + $O_2$] in MeOH, revealing $Co^{III}$-superoxide and high-spin $Co^{II}$ signals. Conditions: 86 mM $H_2Q$, 2 mol% Co(salophen) (1.7 mM), 1 atm $O_2$, MeOH. (B) UV−visible spectra of catalytic reaction mixtures under various pressures of $O_2$ (solid lines) and a reference spectrum for the $Co^{III}$-superoxide species generated at low temperature (dashed line). Conditions: 86 mM $H_2Q$, 1 mol% Co(salophen) (0.8 mM), 1 atm $O_2$, MeOH.

$$4\ Co^{II}(salophen) + O_2 + 4\ MeOH \rightarrow 4\ Co^{III}(salophen)(OMe) + 2\ H_2O \quad (2)$$

Autoxidation of $Co^{II}$(salophen) under aerobic conditions is evident by UV−visible spectroscopy. Bubbling $O_2$ through a MeOH solution of $Co^{II}$(salophen) results in a new absorption band that appears at 490 nm (Figure 5A). Negligible change is observed upon sparging the solution with $N_2$, consistent with irreversible formation of $Co^{III}$ (Figure 5A; cf. solid red vs dashed black spectra). If $Co^{II}$(salophen) is exposed to $O_2$ at −45 °C, reversible $O_2$ binding is observed (Figure 5B). The spectrum observed following addition of $O_2$ is different from that observed in the autoxidation reaction and exhibits a shoulder at 475 nm. Regeneration of $Co^{II}$(salophen) is observed upon sparging the solution with $N_2$, consistent with reversible formation of a $Co^{III}$-superoxide species.

*UV−Visible and EPR Analysis of $Co^{II}$(salophen) under Aerobic Catalytic Conditions for $H_2Q$ Oxidation.* The Co speciation during catalytic turnover was probed by EPR and UV−visible spectroscopic methods. An aliquot of a catalytic reaction mixture under 1 atm $O_2$ was withdrawn and rapidly transferred to an EPR tube and frozen in liquid nitrogen. The resulting EPR spectrum reveals a $Co^{III}$-superoxide signal identical to that described above (cf. Figure 4A), together with a high-spin $Co^{II}$ signal (Figure 6A). The catalytic reaction was also monitored in situ by UV−visible spectroscopy at different partial pressures of $O_2$ (Figure 6B). Under $N_2$, the spectrum of the catalytic reaction mixture matches the spectrum of $Co^{II}$(salophen). Under $O_2$, an absorbance feature is observed at 475 nm, consistent with the $Co^{III}$-superoxide species (dashed black spectrum, Figure 6B), and its intensity increases for catalytic reactions performed at higher $pO_2$.

**Preliminary Mechanistic Proposal and Consideration of Unanswered Questions.** The kinetic and spectroscopic data described above provide the basis for a preliminary catalytic mechanism, depicted in Scheme 2. The kinetic data show that all three reaction components, Co(salophen), $O_2$, and $H_2Q$, come together in the turnover-limiting step. Step 1 involves reversible binding of $O_2$ to the Co center and is supported by the saturation kinetic dependence of the rate on $pO_2$, EPR spectroscopic evidence for formation of a $Co^{III}$−superoxide species, and UV−visible spectroscopic data showing that the steady-state concentration of the $Co^{III}$−superoxide intermediate varies with $pO_2$ under catalytic conditions.[17−19]



DOI: 10.1021/jacs.6b00254
J. Am. Chem. Soc. 2016, 138, 4186−4193

**Scheme 2. Initial Proposal for Mechanism Based on Kinetic and Spectroscopic Techniques**[a]

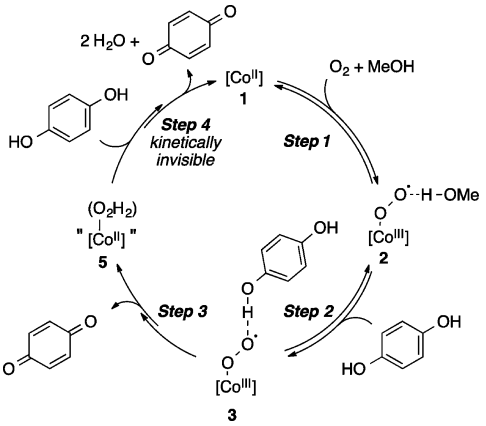


[a][Co] = Co(salophen). The numbering of the intermediates reflects the compound numbers used in the DFT computational studies described below (Scheme 4).

Step 2 features formation of a hydrogen-bonded adduct between $H_2Q$ and the $Co^{III}$-superoxide species, which is invoked to explain the saturation kinetic dependence on $[H_2Q]$.[20] Efforts to obtain direct spectroscopic evidence for this hydrogen-bonding interaction were unsuccessful, probably reflecting the difficulty in distinguishing between a hydrogen bond from MeOH vs $H_2Q$. The large kinetic isotope effect is consistent with turnover-limiting H-atom transfer, which ultimately leads to formation of BQ as the product in Step 3. Steps 1−3 account for formation of the first equivalent of BQ, while another series of steps, collected in Step 4, account for oxidation of the second equivalent of $H_2Q$ to account for the net four-electron reduction of $O_2$ to $H_2O$. These steps are fast relative to the initial activation of $O_2$ and oxidation of the first $H_2Q$ molecule, and therefore are kinetically and spectroscopically invisible. According to this mechanistic proposal, the beneficial effect of MeOH as a solvent (cf. Figure 1) could be attributed to its ability to stabilize the $Co^{III}$−superoxide intermediate via hydrogen-bonding.[21] Multiple other roles of solvent are also possible, however (e.g., solvent ligation to Co, solvent involvement in proton-transfer steps).

Several possibilities may be considered for (i) the fate of $O_2$ during oxidation of the first equivalent of $H_2Q$ and (ii) the mechanism of oxidation of the second equivalent of $H_2Q$. In Scheme 3, pathway A features activation of $O_2$ by $[Co^{II}]$ and $H_2Q$ to afford a $[Co^{III}]$−oxyl (or $[Co^{IV}]$−oxo), which is expected to be a highly reactive species capable of oxidizing the second equivalent of $H_2Q$. In pathway B, $O_2$ undergoes two-electron reduction to $H_2O_2$, either as a $[Co^{II}]-(O_2H_2)$ adduct or as a free intermediate, and then $H_2O_2$ oxidizes the second equivalent of $H_2Q$. Finally, in pathway C, $H_2O_2$ forms as an intermediate and then undergoes rapid (Co-catalyzed) disproportionation into $1/2\ O_2$ and $H_2O$.[22] In this case, oxidation of the second equivalent of $H_2Q$ proceeds via the same aerobic pathway as the first equivalent.

**Assessing the Potential Involvement of $H_2O_2$ Disproportionation (Scheme 3, Pathway C).** It was possible to test pathway C in Scheme 3 experimentally. $H_2O_2$·urea was used as a convenient source of anhydrous $H_2O_2$. Control experiments revealed that urea has minimal effect on catalytic aerobic oxidation of $H_2Q$[23] and that $H_2O_2$ is not an effective oxidant of $H_2Q$ in the absence of Co(salophen). $H_2O_2$ was found to undergo disproportionation in the presence of Co(salophen) under anaerobic conditions in the absence of $H_2Q$. The rate of this process, however, was more than 2-fold slower than the rate of catalytic $H_2Q$ oxidation under otherwise identical conditions (Figure 7, blue vs black trace). Separate experiments showed that $H_2O_2$ served as an effective terminal oxidant in Co(salophen)-catalyzed oxidation of $H_2Q$ to BQ (i.e., in the absence of $O_2$). Only small amounts of $O_2$ evolution were observed under these conditions (Figure 7, red trace). Together, these results provide evidence against pathway C in Scheme 3 and suggest that, if hydrogen peroxide forms, it will oxidize $H_2Q$ in preference to undergoing disproportionation.

**Scheme 3. Possible Fates of $O_2$ during Oxidation of the First Equivalent of $H_2Q$ (i) and Possible Pathways for Oxidation of the Second Equivalent of $H_2Q$ (ii)**

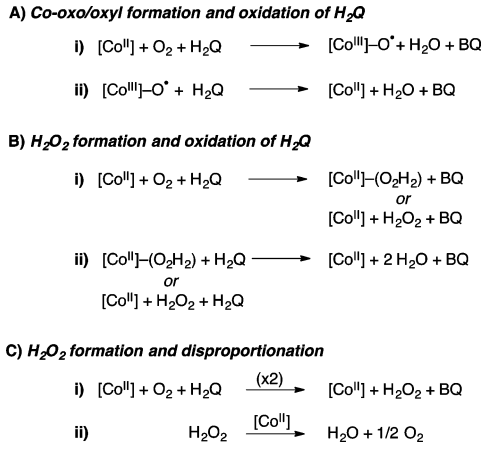


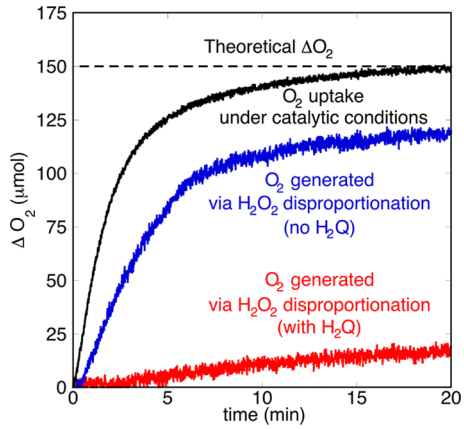


**Figure 7.** Comparison of Co(salophen)-catalyzed aerobic oxidation of $H_2Q$ (black) to the rate of Co(salophen)-catalyzed disproportionation of $H_2O_2$ in the absence and presence of $H_2Q$ (blue and red, respectively). Conditions: 2.5 mM Co(salophen), 86 mM $H_2Q$, 0.3 mmol $H_2O_2$·urea injected over 5 min via syringe pump.

**DFT Analysis of Likely Pathway for Co(salophen)-Catalyzed $H_2Q$ Oxidation.** DFT computational studies provided a means to compare pathways A and B, specifically to assess the relative free energies of formation of a Co-oxo/oxyl species versus hydrogen peroxide. In addition to probing this specific question, a full sequence of intermediates and key transition states involved in the oxidation of 2 equiv of $H_2Q$ was analyzed (Scheme 4). The experimental data provided


DOI: 10.1021/jacs.6b00254
J. Am. Chem. Soc. 2016, 138, 4186−4193

**Scheme 4. Free-Energy Diagram of $Co^{II}$(salophen)-Catalyzed Aerobic Oxidation of $H_2Q$ in Methanol Involving a $Co^{III}$–Oxyl (6a, Pathway A) or $Co^{II}$–($O_2H_2$) (6, Pathway B) Intermediate[a]**

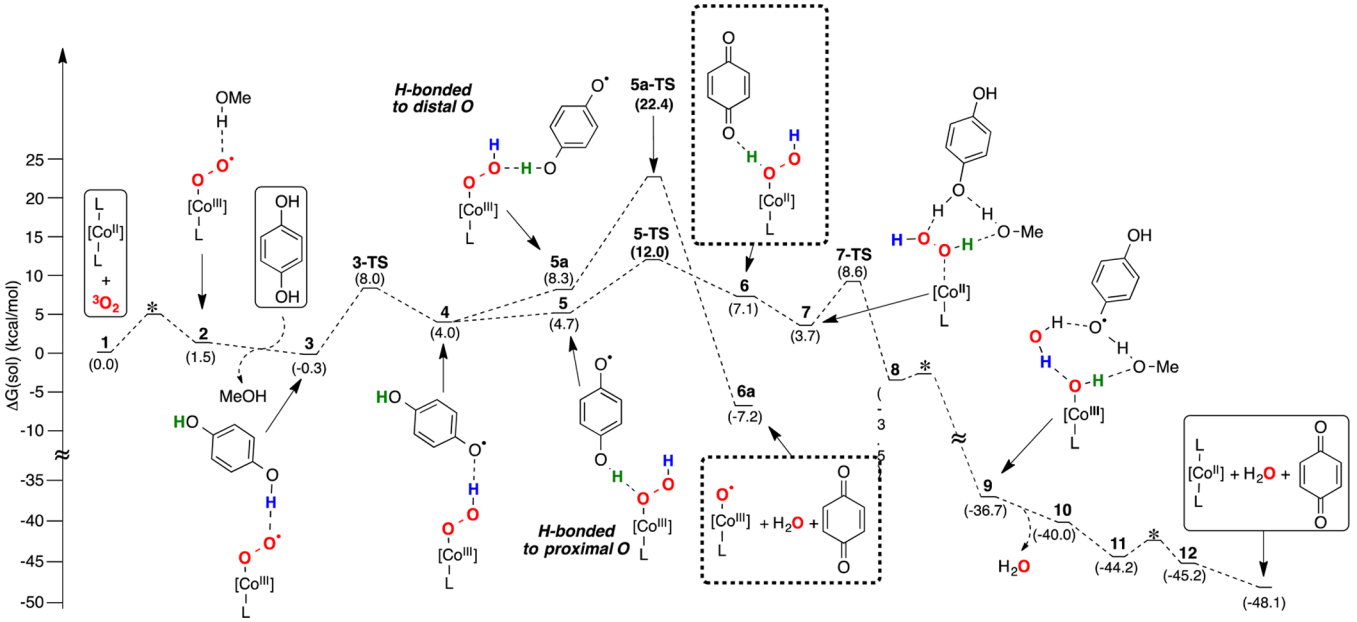


[a][Co] = Co(salophen), L = MeOH (see Supporting Information for full details).

important benchmarks, especially for oxidation of the first equivalent of $H_2Q$.

Dioxygen binding is calculated to be 1.5 kcal/mol uphill in free energy from the bis-methanol adduct of $Co^{II}$(salophen) and features significant charge transfer from the metal center to dioxygen. Mulliken Spin Density analysis suggests that this complex (**2**) is best represented as a $Co^{III}$–superoxo species. Hydrogen bonding of $H_2Q$ decreases the overall free energy by 1.8 kcal/mol (cf. complex **3**).[21] The similar free energies calculated for structures **1**–**3** align with the experimental data described above, which provided evidence for each of these species prior to the rate-limiting step in the oxidation of $H_2Q$.

H-atom transfer from $H_2Q$ to the terminal oxygen of $Co^{III}(O_2^{\bullet})$ forms the protonated semiquinone ($SQH^{\bullet}$) adduct **4**. This step is endergonic by 4.3 kcal/mol and exhibits an activation free energy barrier of 8.3 kcal/mol (**3-TS**). The free energy diagram in Scheme 4 then branches at structure **4** into the two pathways, one leading to cleavage of the O–O bond of dioxygen (pathway A via **5a-TS** in Scheme 4) and the other forming hydrogen peroxide (pathway B via **5-TS** in Scheme 4). Both pathways require rearrangement of the H-bonding network between $SQH^{\bullet}$ and $Co^{III}(O_2H)$. In pathway A, a H-bonded complex (**5a**) forms between $SQH^{\bullet}$ and the distal oxygen of the $Co^{III}(O_2H)$ species, followed by exergonic PCET to afford water and the $Co^{III}(O^{\bullet})$ species **6a**. Pathway B is initiated by formation of a different H-bonded complex (**5**), in which the $SQH^{\bullet}$ interacts with the proximal oxygen of the $Co^{III}(O_2H)$ species, and subsequent PCET affords the coordinated $H_2O_2$ adduct **6**. Though formation of $Co^{III}(O^{\bullet})$ **6a** is thermodynamically favored by >14 kcal/mol relative to **6**, the free energy of the transition state en route to **6a** is 10.4 kcal/mol higher than that leading to **6**. Moreover, the calculated free energy of **5a-TS** relative to the initial reactants (22.4 kcal/mol) is significantly higher than the effective activation barrier for the catalytic reaction estimated from the experimental reaction rate (~13.6 kcal/mol, see Supporting Information for details). In contrast, the transition state for formation of the $H_2O_2$ adduct **6** exhibits a calculated free energy of 12.0 kcal/mol relative to the initial reactants, which is quite similar to the experimental estimate.

According to the calculations, the transition state associated with transfer of the second hydrogen atom via **5-TS** has the highest free energy along reaction pathway B. The KIE for this pathway was calculated from the differences in the H versus D zero point energies for **5-TS**/methanol and **1**/$H_2Q$.[24] The calculated KIE of 4.1 is nearly identical to the experimental KIE.[25,26] This agreement between the calculated and experimental KIE aligns with the good agreement between the calculated and experimental reaction barriers noted above, and together they provide strong support for pathway B.

Pathways A and B exhibit different types of transition states following intermediate **4**. In pathway A, transition state **5a-TS** exhibits a significant increase in the O–O bond length relative to **5a** (from 1.44 Å in **5a** to 1.76 Å in **5a-TS**), and the spin density on the $SQH^{\bullet}$ decreases from 1.0 to 0.7, while the spin density on the proximal oxygen atom increases from 0.0 to 0.2. These changes reflect a significant charge redistribution in the TS. In pathway B, formation of the $Co^{II}$-($O_2H_2$) adduct **6** from **5** is best described as a PCET step, with proton delivery to the proximal oxygen of the $Co^{III}(O_2H)$ species and electron transfer to $Co^{III}$. Mulliken Spin Density analysis at the TS indicates that the distribution of electron density is reactant-like, with the O–O bond lengthening only from 1.43 Å in **5** to 1.44 Å in **5-TS** [cf. $d_{O-O}$(**6**) = 1.46 Å].

All steps beyond **5-TS** in Scheme 4 are lower in free energy than this transition state, and a viable pathway for Co(salophen)-catalyzed oxidation of the second equivalent of $H_2Q$ by $H_2O_2$ was identified (cf. species **7**–**12** in Scheme 4). The computations suggest that this second oxidation step is necessary to drive the reaction because the oxidation of hydroquinone to benzoquinone with $O_2$ reduction to $H_2O_2$ is slightly uphill thermodynamically. Hydrogen peroxide is not expected to be a good ligand (cf. **6** and **7**),[27] but involvement of a Co–($O_2H_2$) adduct in $H_2Q$ oxidation is consistent with the


DOI: 10.1021/jacs.6b00254
J. Am. Chem. Soc. 2016, 138, 4186–4193

control experiments showing that kinetically competent oxidation of $H_2Q$ by $H_2O_2$ requires Co(salophen).

## CONCLUSIONS

In summary, the experimental and computational results presented above illuminate the pathway for Co(salophen)-catalyzed aerobic oxidation of *p*-hydroquinone. Molecular oxygen is unreactive with $H_2Q$ in the absence of $Co^{II}$(salophen); however, reductive activation of $O_2$ by $Co^{II}$ leads to formation of a $Co^{III}$-superoxide species that promotes facile H-atom abstraction from $H_2Q$. Proton-coupled electron-transfer between the resulting semiquinone ($SQH^{\bullet}$) and $Co^{III}$-OOH intermediates is the turnover-limiting step of the overall catalytic reaction and completes the oxidation of the first equivalent of $H_2Q$. $Co^{II}$(salophen) then catalyzes rapid oxidation of a second equivalent of $H_2Q$ using the $H_2O_2$ generated in the first oxidation process.

Co(salophen)-catalyzed aerobic oxidation of $H_2Q$ involves efficient four-electron reduction of $O_2$ to $H_2O$ without the accumulation of partially reduced oxygen intermediates, such as superoxide or hydrogen peroxide. The avoidance of such reactive oxygen species in the four-electron reduction of $O_2$ potentially accounts for the importance of the Co(salophen)/BQ co-catalyst system in Pd- and other metal-catalyzed aerobic oxidation reactions. In effect, $H_2Q$ serves as an "anti-oxidant" to prevent deleterious side reactions from $O_2$-derived species, and BQ is generated as an effective oxidant for the metal-catalyzed oxidation of the organic substrate (cf. Scheme 1).

## ASSOCIATED CONTENT

### Supporting Information

The Supporting Information is available free of charge on the ACS Publications website at DOI: 10.1021/jacs.6b00254.

Experimental details for data acquisition, additional kinetic data, computational details, and coordinates of computed structures (PDF)

## AUTHOR INFORMATION


### Corresponding Authors

*shs3@illinois.edu

*stahl@chem.wisc.edu


### Notes

The authors declare no competing financial interest.

## ACKNOWLEDGMENTS

This research was supported as part of the Center for Molecular Electrocatalysis, an Energy Frontier Research Center, funded by the U.S. Department of Energy, Office of Science, Office of Basic Energy Sciences. The NSF provided partial support for the EPR instrumentation (NSF CHE-0741901).

## REFERENCES


(1) For representative reviews, see: (a) Stahl, S. S. *Angew. Chem., Int. Ed.* **2004**, *43*, 3400−3420. (b) Punniyamurthy, T.; Velusamy, S.; Iqbal, J. *Chem. Rev.* **2005**, *105*, 2329−2363. (c) Piera, J.; Bäckvall, J.-E. *Angew. Chem., Int. Ed.* **2008**, *47*, 3506−3523. (d) Wendlandt, A. E.; Suess, A. M.; Stahl, S. S. *Angew. Chem., Int. Ed.* **2011**, *50*, 11062−11087. (e) Shi, Z.; Zhang, C.; Tang, C.; Jiao, N. *Chem. Soc. Rev.* **2012**, *41*, 3381−3430.

(2) Vasseur, A.; Muzart, J.; Le Bras, J. *Eur. J. Org. Chem.* **2015**, *2015*, 4053−4069.

(3) For leading references, see: (a) Morandi, B.; Wickens, Z. K.; Grubbs, R. H. *Angew. Chem., Int. Ed.* **2013**, *52*, 2944−2948. (b) Bäckvall, J.-E.; Hopkins, R. B.; Grennberg, H.; Mader, M. M.; Awasthi, A. K. *J. Am. Chem. Soc.* **1990**, *112*, 5160−5166. (c) Purse, B. W.; Tran, L.-H.; Piera, J.; Åkermark, B.; Bäckvall, J.-E. *Chem. - Eur. J.* **2008**, *14*, 7500−7503. (d) Gigant, N.; Bäckvall, J.-E. *Chem. - Eur. J.* **2014**, *20*, 5890−5894. (e) Volla, C. M. R.; Bäckvall, J.-E. *Org. Lett.* **2014**, *16*, 4174−4177.

(4) (a) Bäckvall, J.-E.; Chowdhury, R. L.; Karlsson, U. *J. Chem. Soc., Chem. Commun.* **1991**, 473−475. (b) Samec, J. S. M.; Éll, A. H.; Bäckvall, J.-E. *Chem. - Eur. J.* **2005**, *11*, 2327−2334. (c) Largeron, M. *Eur. J. Org. Chem.* **2013**, *2013*, 5225−5235. (d) Wendlandt, A. E.; Stahl, S. S. *Angew. Chem., Int. Ed.* **2015**, *54*, 14638−14658.

(5) Sazanov, L. A. *Nat. Rev. Mol. Cell Biol.* **2015**, *16*, 375−388.

(6) See, for example: Gerken, J. B.; Stahl, S. S. *ACS Cent. Sci.* **2015**, *1*, 234−243.

(7) (a) Tyson, C. A.; Martell, A. E. *J. Am. Chem. Soc.* **1972**, *94*, 939−945. (b) Sakamoto, H.; Funabiki, T.; Yoshida, S.; Tarama, K. *Bull. Chem. Soc. Jpn.* **1979**, *52*, 2760−2765. (c) Tsuruya, S.; Yanai, S.-i.; Masai, M. *Inorg. Chem.* **1986**, *25*, 141−146. (d) Simándi, L. I.; Barna, T.; Argay, G.; Simándi, T. L. *Inorg. Chem.* **1995**, *34*, 6337−6340. (e) Simándi, L. I.; Simándi, T. L. *J. Chem. Soc., Dalton Trans.* **1998**, 3275−3279. (f) Simándi, T. L.; Simándi, L. I. *React. Kinet. Catal. Lett.* **1998**, *65*, 301−309. (g) Simándi, T. M.; May, Z.; Szigyártó, I. C.; Simándi, L. I. *Dalton Trans.* **2005**, 365−368.

(8) For reports of cobalt-catalyzed aerobic oxidation of *p*-hydroquinone, see: (a) Abel, E. W.; Pratt, J. M.; Whelan, R.; Wilkinson, P. J. *J. Am. Chem. Soc.* **1974**, *96*, 7119−7120. (b) Németh, S.; Szeverényi, Z.; Simándi, L. I. *Inorg. Chim. Acta* **1980**, *44*, L107−L109. (c) Volpin, M. E.; Jáky, M.; Kolosova, E. M.; Tuvin, M. Y.; Novodarova, G. N. *React. Kinet. Catal. Lett.* **1982**, *21*, 41−44. (d) Sakata, K.; Kikutake, T.; Shigaki, Y.; Hashimoto, M. *Inorg. Chim. Acta* **1988**, *144*, 1−3. (e) Yakubovich, T. N.; Ermokhina, N. I.; Bratushko, Y. I.; Zub, Y. L.; Chuiko, A. A. *Kinet. Catal.* **1993**, *33*, 688−693. (f) Jäger, E.-G.; Knaudt, J.; Rudolph, M.; Rost, M. *Chem. Ber.* **1996**, *129*, 1041−1047.

(9) Hartl, F.; Vlček, A., Jr. *Inorg. Chim. Acta* **1986**, *118*, 57−63.

(10) For reviews discussing H-atom transfer, and proton-coupled electron transfer generally, see: (a) Huynh, M. H. V.; Meyer, T. J. *Chem. Rev.* **2007**, *107*, 5004−5064. (b) Hammes-Schiffer, S.; Stuchebrukhov, A. A. *Chem. Rev.* **2010**, *110*, 6939−6960. (c) Warren, J. J.; Tronic, T. A.; Mayer, J. M. *Chem. Rev.* **2010**, *110*, 6961−7001.

(11) The −OH bonds of hydroquinone were assumed to exchange with deuterated solvent to yield hydroquinone-$d_2$.

(12) Vinck, E.; Carter, E.; Murphy, D. M.; Van Doorslaer, S. *Inorg. Chem.* **2012**, *51*, 8014−8024. Further discussion is presented in the Supporting Information.

(13) Walker, F. A. *J. Am. Chem. Soc.* **1970**, *92*, 4235−4244.

(14) Numerous examples are included in the following review articles: (a) McLendon, G.; Martell, A. E. *Coord. Chem. Rev.* **1976**, *19*, 1−39. (b) Jones, R. D.; Summerville, D. A.; Basolo, F. *Chem. Rev.* **1979**, *79*, 139−179. (c) Niederhoffer, E. C.; Timmons, J. H.; Martell, A. E. *Chem. Rev.* **1984**, *84*, 137−203.

(15) Nishinaga, A.; Kondo, T.; Matsuura, T. *Chem. Lett.* **1985**, 905−908.

(16) For autoxidation of other $Co^{II}$ complexes in methanol, see: (a) Simándi, L. I.; Savage, C. R.; Schelly, Z. A.; Németh, S. *Inorg. Chem.* **1982**, *21*, 2765−2769. (b) Pavlović, D.; Ašperger, S.; Dokuzović, Z.; Jurišić, B.; Ahmeti, X.; Sertić, M.; Murati, I. *J. Chem. Soc., Dalton Trans.* **1985**, 1095−1101.

(17) Equilibrium binding of $O_2$ to macrocyclic $Co^{II}$ species has been the subject of considerable historical investigation, as documented in the reviews in ref 14. For $O_2$-binding equilibrium constants at low temperature in MeOH, see ref 18, and for $O_2$ binding to $Co^{II}$(salophen) in an aprotic solvent (diglyme) at room temperature, see ref 19. The latter reaction is nearly thermoneutral: under 1 atm $O_2$, [$Co^{III}$-superoxide]/[$Co^{II}$] = 1.4

(18) (a) Carter, M. J.; Engelhardt, L. M.; Rillema, D. P.; Basolo, F. *J. Chem. Soc., Chem. Commun.* **1973**, 810−812. (b) Rillema, D. P.; Wicker, C. M.; Morgan, R. D. *J. Phys. Chem.* **1983**, *87*, 5151−5158.




DOI: 10.1021/jacs.6b00254
*J. Am. Chem. Soc.* 2016, 138, 4186−4193

(19) Chen, D.; Martell, A. E. *Inorg. Chem.* **1987**, *26*, 1026−1030.
(20) A similar mechanism has been proposed for the H-atom abstraction from phenols by a mononuclear $Mn^{III}(OH)$ species and is supported by a saturation kinetic dependence on [phenol]: Wijeratne, G. B.; Corzine, B.; Day, V. W.; Jackson, T. A. *Inorg. Chem.* **2014**, *53*, 7622−7634.
(21) The ability of intermolecular or intramolecular hydrogen bonding to favor $O_2$ binding to $Co^{II}$ has been discussed elsewhere: (a) Drago, R. S.; Cannady, J. P.; Leslie, K. A. *J. Am. Chem. Soc.* **1980**, *102*, 6014−6019. (b) Collman, J. P.; Zhang, X.; Wong, K.; Brauman, J. I. *J. Am. Chem. Soc.* **1994**, *116*, 6245−6251.
(22) For a study of Co-macrocycle-catalyzed disproportionation of $H_2O_2$, see: Waldmeier, P.; Prijs, B.; Sigel, H. *Z. Naturforsch., B: J. Chem. Sci.* **1972**, *27*, 95−100.
(23) The rate of $H_2Q$ oxidation in the presence of 1 equiv of urea is 80% of that in the absence of urea. See Figure S9 for further details.
(24) Kozuch, S.; Shaik, S. *Acc. Chem. Res.* **2011**, *44*, 101−110.
(25) Experimental kinetic studies suggest that the catalyst resting state is an equilibrium mixture of species **1**, **2**, and **3**. The calculated KIE of **5-TS** relative to **3** is 4.5, which is also in agreement with the experimental KIE.
(26) The computed KIE for pathway A (through **5a-TS**) is 3.7. The KIE values do not distinguish between the two pathways; however, the relative free energies of **5-TS** and **5a-TS** are able to distinguish between the two pathways.
(27) See, for example: (a) Mirza, S. A.; Bocquet, B.; Robyr, C.; Thomi, S.; Williams, A. F. *Inorg. Chem.* **1996**, *35*, 1332−1337. (b) DiPasquale, A. G.; Mayer, J. M. *J. Am. Chem. Soc.* **2008**, *130*, 1812−1813.


DOI: 10.1021/jacs.6b00254
*J. Am. Chem. Soc.* 2016, 138, 4186−4193